

32 GHz high-power MUTC waveguide photodiode for 1310 nm

Fengxin Yu, Keye Sun, Junyi Gao, and Andreas Beling

Department of Electrical and Computer Engineering, University of Virginia, Charlottesville, VA 22904, USA
fy6uq@virginia.edu

Abstract: We demonstrate evanescently coupled modified uni-traveling carrier (MUTC) waveguide photodiodes for 1310 nm wavelength with saturation photocurrent >20 mA and high radio frequency (RF) output power of 5.7 dBm at 30 GHz.

OCIS codes: (230.5170) Photodiodes, (060.5625) Radio frequency photonics

1. Introduction

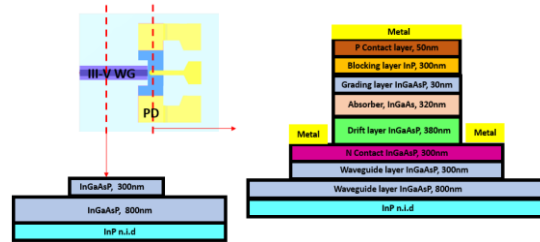
High-power high-speed waveguide photodiodes (PDs) continue to be critical components in optical systems and analog photonics applications that require integrated high-linearity photodetectors on chip. For example, microwave photonics applications such as low-phase-noise microwave signal generation, antenna remoting, and radio-over-fiber benefit from high power handling capability of the PD to maintain high RF gain and large spurious-free dynamic range [1-3]. Whereas much progress has been reported for high-power photodiodes at 1550 nm wavelength (e.g. [4, 5]), to date only few high-speed waveguide PDs with photocurrents up to 13 mA have been demonstrated for detection at 1310 nm [6, 7].

In this paper, we report on high-power evanescently coupled waveguide MUTC PDs that have a 3 dB-bandwidth of 32 GHz, high responsivity, and provide photocurrents > 20 mA. The PDs have an unsaturated RF output power of 5.7 dBm at 30 GHz which we believe is the highest output power that has been reported in this frequency range for waveguide PDs at 1310 nm.

2. Design and Fabrication

P Contact layer, InGaAs, p+, Zn, $1 \times 10^{19} \text{ cm}^{-3}$, 50nm
Blocking layer, InP, p+, Zn, $2 \times 10^{18} \text{ cm}^{-3}$, 300nm
Grading, InGaAsP, Q1.1, p+, Zn, $2 \times 10^{18} \text{ cm}^{-3}$, 15nm
Grading, InGaAsP, Q1.4, p+, Zn, $2 \times 10^{18} \text{ cm}^{-3}$, 15nm
Absorber, In _{0.53} Ga _{0.47} As, p+, Zn, $5 \times 10^{18} \text{ cm}^{-3}$, 30nm
Absorber, InGaAs, p+, Zn, $3 \times 10^{18} \text{ cm}^{-3}$, 30nm
Absorber, InGaAs, p+, Zn, $1 \times 10^{19} \text{ cm}^{-3}$, 40nm
Absorber, InGaAs, p, Zn, $8 \times 10^{17} \text{ cm}^{-3}$, 40nm
Absorber, InGaAs, p, Zn, $7 \times 10^{17} \text{ cm}^{-3}$, 40nm
Absorber, InGaAs, p, Zn, $6 \times 10^{17} \text{ cm}^{-3}$, 40nm
Depleted Absorber, InGaAs, n, Si, $1 \times 10^{16} \text{ cm}^{-3}$, 100nm
Grading, InGaAsP, Q1.53, Si, $1 \times 10^{16} \text{ cm}^{-3}$, 15nm
Grading, layer InGaAsP, Q1.4, Si, $1 \times 10^{16} \text{ cm}^{-3}$, 15nm
Charge layer InGaAsP, Q1.2 n, Si, $1 \times 10^{17} \text{ cm}^{-3}$, 50nm
Drift layer InGaAsP, Q1.1 n, Si, $1 \times 10^{16} \text{ cm}^{-3}$, 300nm
N Contact InGaAsP, Q1.1, n+, Si, $1 \times 10^{19} \text{ cm}^{-3}$, 300nm
Waveguide rib InGaAsP, Q1.1, n.i.d. 300nm
Waveguide layer InGaAsP, Q1.1, n.i.d. 800nm
InP n.i.d.

(a)



(b)

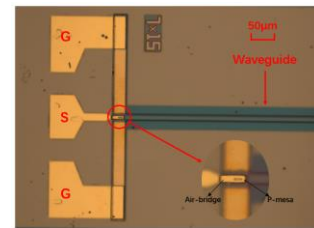


Fig. 2. Top-view of a fabricated waveguide PD with ground (G)-signal (S)-ground (G) RF probe pad.

Fig. 1. Epitaxial layer structure (a) and cross sections (b) of the waveguide PD. All layers are lattice-matched to InP.

Fig. 1a shows the epitaxial layer structure of the waveguide PD. The structure was grown on semi-insulating InP substrate by metal organic chemical vapor deposition and in situ-doped with zinc (p-type) and silicon (n-type) dopants. The design includes a 1.1 μm -thick undoped wide-bandgap InGaAsP waveguide layer followed by the 300 nm-thick heavily n-type doped InGaAsP contact layer. The 300 nm-thick electron drift layer was grown with a light n-type doping ($1 \times 10^{16} \text{ cm}^{-3}$) for charge compensation and is followed by a 50 nm n-type doped ($1 \times 10^{17} \text{ cm}^{-3}$) charge layer. We have previously shown that this charge layer can help to reduce the deleterious effect of space charge at high photocurrents and thus increase the output power of the PD [8]. The fact that we designed the n-contact, drift, and

charge layers with wider bandgaps than their counterparts in a waveguide PD for 1550 nm [4] had no significant impact on the PD's responsivity. In order to suppress charge accumulation at the heterojunction interfaces, two 15 nm-thick lightly n-type doped InGaAsP layers were grown. For high efficiency, we adopted 320 nm-thick InGaAs as the absorber. The absorber layer includes a carefully designed 220 nm graded doping which results in a high built-in electric field for electron acceleration and a 100 nm depleted absorber to improve quantum efficiency [9]. To block electrons from diffusing to the p-type contact layer and to assist hole collection, two 15 nm-thick InGaAsP layers and a 300 nm heavily p-type doped InP layer are included between the absorber layer and the 50 nm-thick heavily p-type doped InGaAs contact layer.

We used a double mesa etching process together with a rib waveguide dry-etching process to fabricate the waveguide PDs. After Ti/Pt/Au p-metal deposition, the p-mesa was etched using a self-aligned etching technique that was stopped at the n-contact layer. Then, the n-mesa followed by the 300-nm waveguide rib were formed by dry-etching (Fig. 1b). Another 800 nm-deep dry-etch was used to define the waveguide. AuGe/Ni/Au were deposited on the n-mesa for n-metal contacts. As shown in Fig. 2, the PDs were connected to gold-plated coplanar waveguide RF pads through an air-bridge. After fabrication, the wafer was cleaved to expose the waveguide facets for light input coupling.

3. Experimental Results

Fig. 3 shows typical I-V curves with dark currents below 500 nA at 5 V reverse bias. The external (fiber-coupled) responsivities were measured using a single-mode tapered optical fiber for input coupling and include the fiber-chip mode mismatch loss and the reflection loss at the photodiode waveguide facet (no anti-reflection coating was used). The external responsivity of waveguide PDs with an active area of $10 \times 15 \mu\text{m}^2$ was 0.28 A/W. In order to determine the internal responsivity, the coupling loss between the tapered fiber and the waveguide was estimated using a commercial

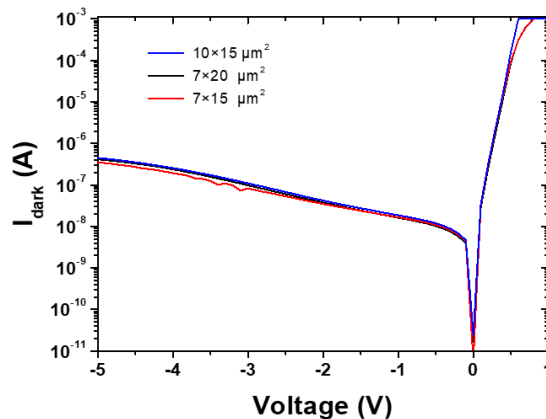


Fig. 3. Measured dark currents of waveguide PDs.

software. Assuming a mode mismatch loss of 3 dB and 1.4 dB reflection loss at the waveguide facet, the internal responsivity is estimated to be as high as 0.77 A/W which corresponds to an external quantum efficiency of 72 % at the 1310 nm wavelength. An optical heterodyne setup with an optical modulation depth close to 100 % was used to characterize the bandwidth and saturation characteristics. The frequency responses of waveguide PDs with various active areas are shown in Fig. 4. Waveguide photodiodes with active areas of $7 \times 20 \mu\text{m}^2$ and $10 \times 15 \mu\text{m}^2$ had bandwidths of 31 GHz and 32 GHz at -5 V, respectively, which suggests that these PDs were not primarily limited by resistance-capacitance (RC) time constant. Also, the $10 \times 15 \mu\text{m}^2$ PD reached its maximum bandwidth of 31 GHz at -3 V which indicates that the drift layer can be fully depleted at this voltage. As shown in Fig. 5, the RF saturation was characterized by measuring the RF output power as a function of the average photocurrent at 30 GHz. The output RF power increases super-linearly with increasing photocurrent before it begins to saturate. We defined the saturation current as the photocurrent where the RF power compression curve drops by 1 dB from its peak value. At -5 V, waveguide PDs with an active area of $10 \times 15 \mu\text{m}^2$ achieved 4.9 dBm output power and the saturation current was 19.8 mA. Waveguide PDs with $7 \times 15 \mu\text{m}^2$ and $7 \times 20 \mu\text{m}^2$ reached 5.7 dBm at 23 mA and 5.3 dBm at 21.3 mA, respectively. It should be noted that these PDs were not yet fully saturated and achieved high RF output power at a reverse of only -3 V bias.

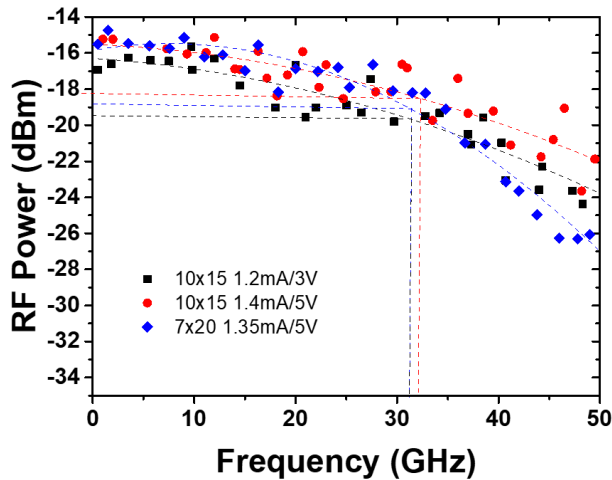


Fig. 4. Measured frequency responses at 1310 nm of waveguide PDs with different active areas.

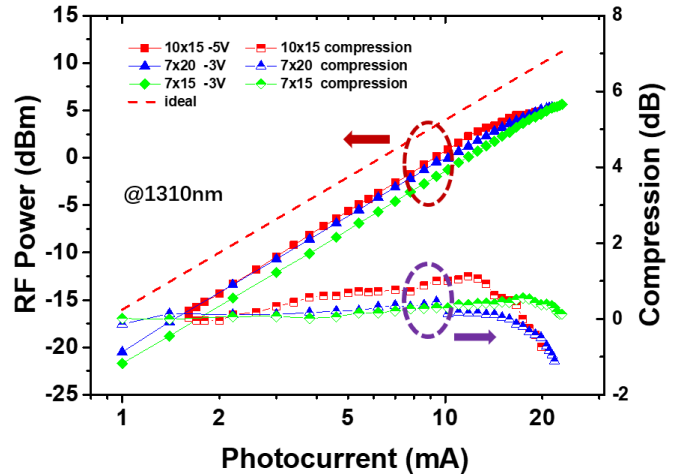


Fig. 5. RF output power and RF power compression versus average photocurrent at 30 GHz. The dashed line represents the ideal RF power at 50 Ω .

4. Summary

High-power evanescently coupled waveguide MUTC photodiodes for 1310 nm wavelength have been successfully fabricated and characterized. The photodiodes have 32 GHz bandwidth, 0.77 A/W responsivity, large un-saturated photocurrent of >20 mA, and 5.7 dBm RF output power at 30 GHz at -3 V. The results show that the devices are well suited for high-power high-speed applications in the O-band.

5. References

- [1] C.H. Cox, E.I Ackerman, G.E. Betts, J.L. Prince, "Limits on the Performance of RF-Over-Fiber Links and Their Impact on Device Design," *IEEE Trans. Microw. Theory Tech.* 2006, 54, 906–920.
- [2] J. Bai, S. Shi, G.J Schneider, J.P. Wilson, Y. Zhang, W. Pan, D.W. Prather, "Optically Driven Ultrawideband Phased Array with an Optical Interleaving Feed Network," *IEEE Antennas Wirel. Propag. Lett.* 2014, 13, 47–50.
- [3] F.N. Baynes, F. Quinlan, T.M. Fortier, Q. Zhou, A. Beling, J.C. Campbell, S.A. Diddams, "Attosecond timing in optical-to-electrical conversion," *Optica* 2015, 2, 141–146.
- [4] Q. Li, K. Sun, K. Li, Q. Yu, P. Runge, W. Ebert, A. Beling, and J. C. Campbell, "High-Power Evanescently Coupled Waveguide MUTC Photodiode With >105 -GHz Bandwidth," *Journal of Lightwave Technology*, vol. 35, no. 21, pp. 4752–4757, Jan. 2017.
- [5] Gan Zhou, Patrick Runge, Shahram Keyvaninia, Sten Seifert, Willi Ebert, Sven Mutschall, Angela Seeger, Qinglong Li, and Andreas Beling, "High-Power InP-Based Waveguide Integrated Modified Uni-Traveling-Carrier Photodiodes," *J. Lightwave Technol.* 35, 717-721 (2017).
- [6] P. Runge, G. Zhou, F. Ganzer, S. Mutschall, and A. Seeger, "Waveguide integrated InP-based photodetector for 100Gbaud applications operating at wavelengths of 1310 nm and 1550 nm", In *2015 European Conference on Optical Communication (ECOC)* (pp. 1-3), IEEE (2015).
- [7] K. Shiba, T. Takeuchi, T. Nakata, K. Makita, K. Fukatsu, T. Kato, and T. Torikai, "A robust 40-Gb/s evanescently coupled waveguide photodiode with high efficiency for use in dual wavelengths: 1310 and 1550-nm," In *Materials, Active Devices, and Optical Amplifiers* (Vol. 5280, pp. 554-559). International Society for Optics and Photonics (2003).
- [8] Z. Li, H. Pan, H. Chen, A. Beling and J. C. Campbell, "High-Saturation-Current Modified Uni-Traveling-Carrier Photodiode With Cliff Layer," in *IEEE Journal of Quantum Electronics*, vol. 46, no. 5, pp. 626-632, May 2010, doi: 10.1109/JQE.2010.2046140.
- [9] D. H. Jun, J. H. Jang, I. Adeseda, and J. I. Song, "Improved efficiency bandwidth product of modified Uni-traveling carrier photodiode structure using an undoped photo-absorption layer," *Jpn. J. Appl. Sci.*, vol. 45, no. 4B, pp. 3475–3478, Apr. 2006.